Supplementary Material

Initiation Timing Improves Retrogressive Thaw Slump Susceptibility Mapping on the Qinghai–Tibet Plateau

Pengfei Li[1,2], Zhuotong Nan[2*], Jiwei Xu[1], Fujun Niu[2]

[1]State Key Laboratory of Climate System Prediction and Risk Management, Nanjing Normal University, Nanjing, 210023, China

[2]Yangtze River Delta Urban Wetland Ecosystem National Field Scientific Observation and Research Station, School of Environmental and Geographical Sciences, Shanghai Normal University, Shanghai, 200234, China

* *Correspondence to*: Zhuotong Nan (nanzt@shnu.edu.cn)

This file includes:

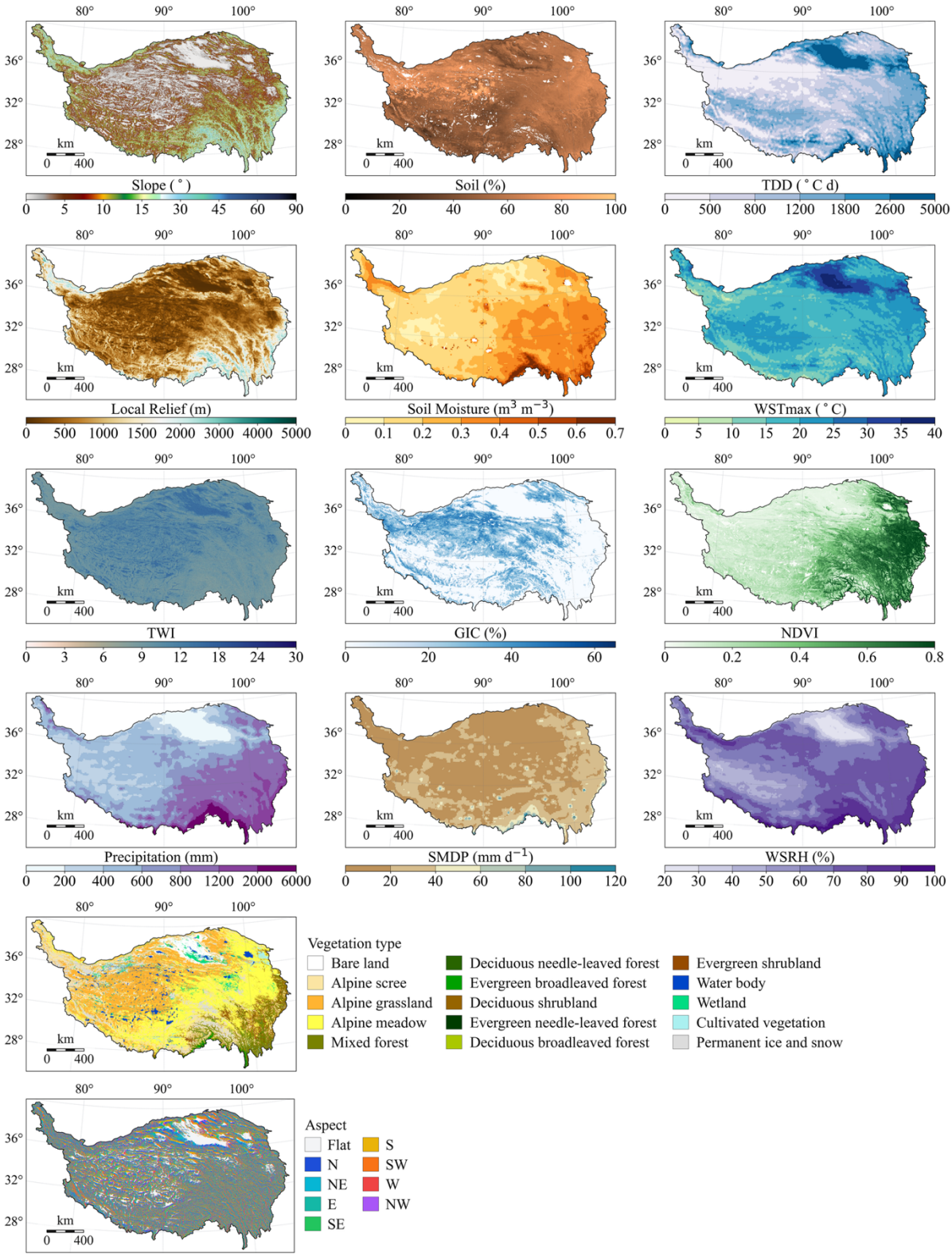

Fig. S1 Spatial distributions of environmental predictors used for RTS susceptibility mapping on the Qinghai–Tibet Plateau. The figure shows the 14 predictors grouped by category: terrain (slope, aspect, TWI, local relief), soil and permafrost (soil fine fraction, ground ice content), vegetation (vegetation type, NDVI), and hydro-climatic variables (TDD, SMDP, precipitation, WSTmax, WSRH, summer soil moisture).

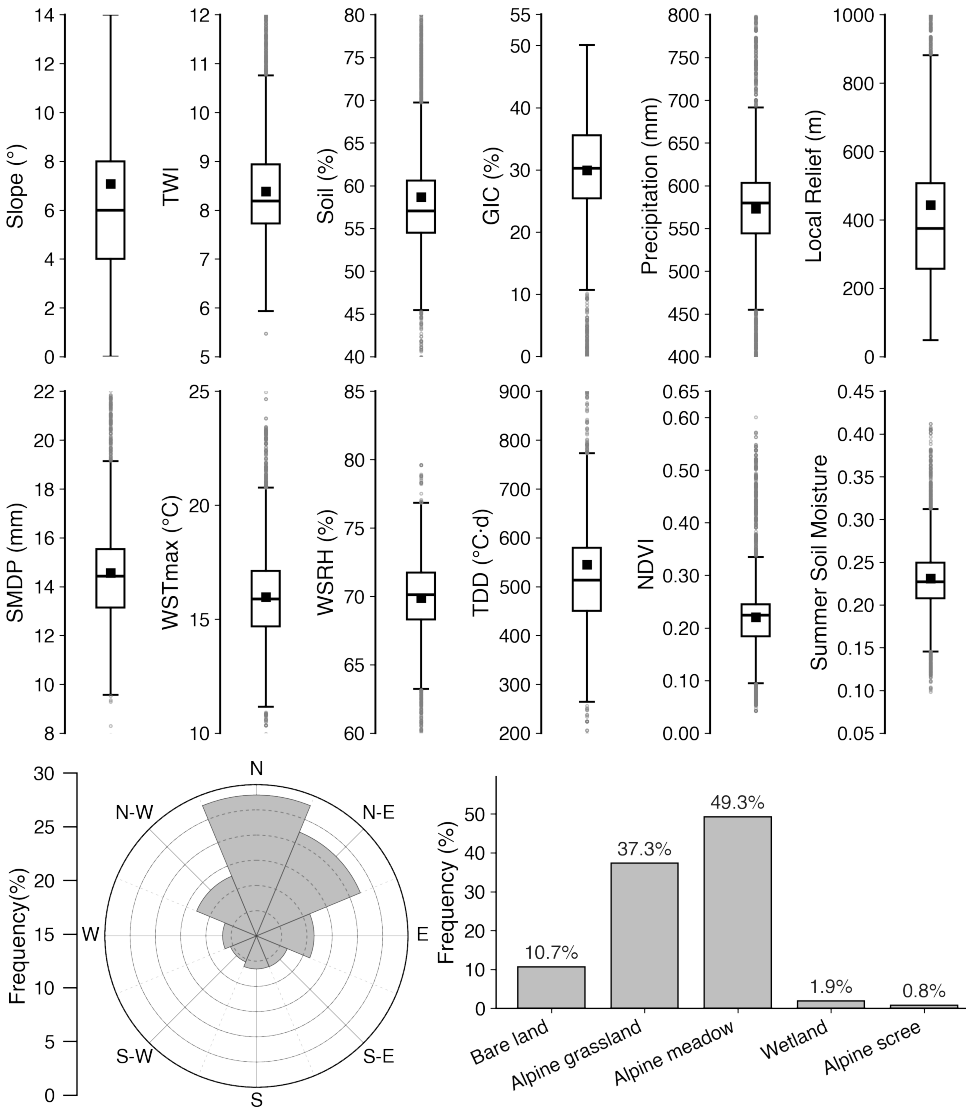

Fig. S2 Distributions of the 14 environmental predictors for RTS positive samples (initiation-year samples) used in model training.

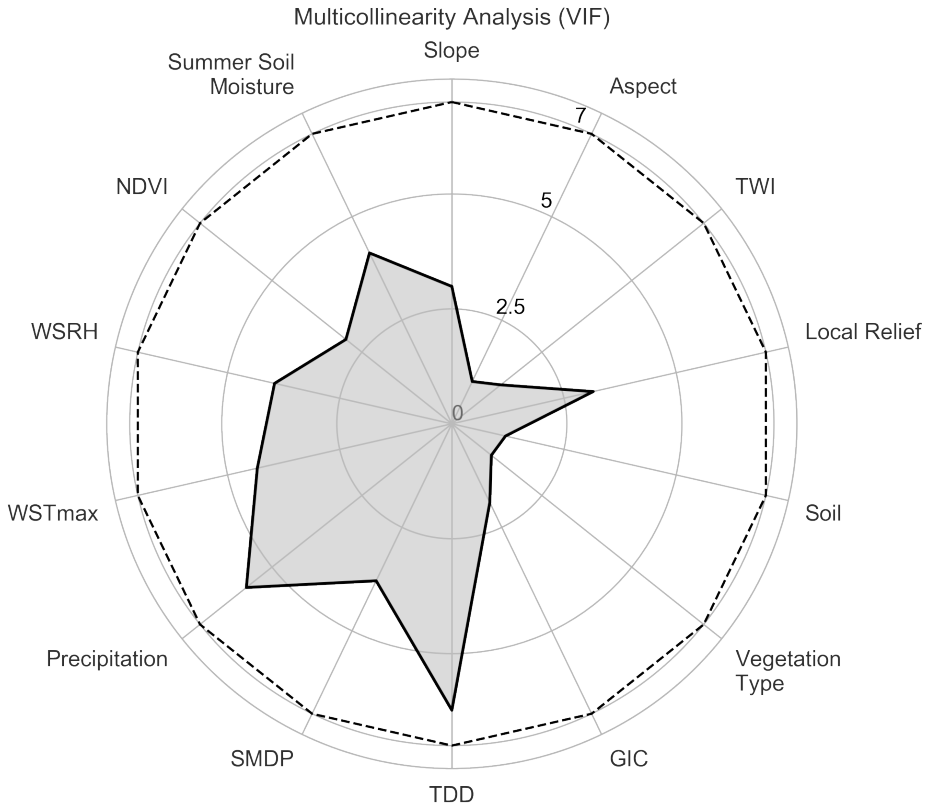

Fig. S3 Variance Inflation Factor (VIF) analysis of the 14 environmental predictors (see Table 1 for full variable definitions). All VIF values are below the commonly used threshold of 7, indicating low multicollinearity among predictors.

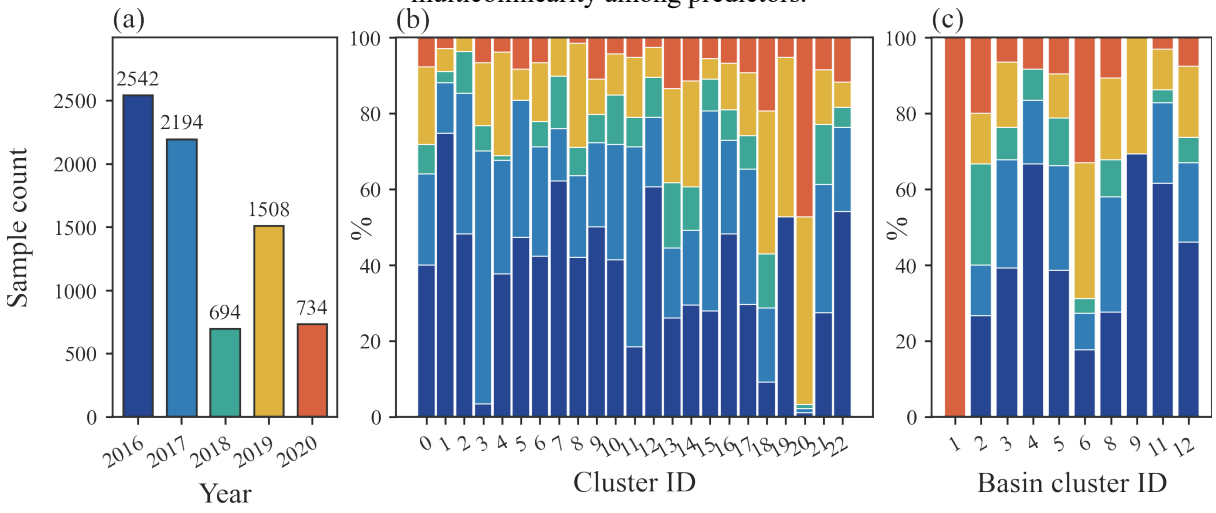

Fig. S4 Sample composition and spatial grouping characteristics of RTS samples from 2016 to 2020. (a) Annual distribution of RTS initiation samples. (b) Distribution of samples among DBSCAN-derived spatial clusters. (c) Distribution of samples among hydrological basin clusters. Colors indicate the proportion of samples originating from different years within each cluster.

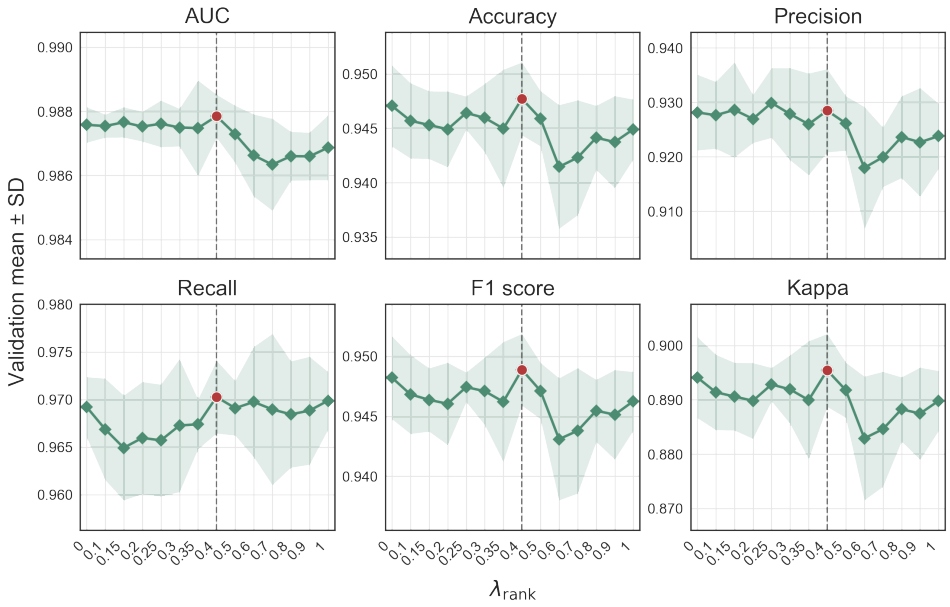

Fig. S5 Sensitivity of five-fold cross-validation performance to the ranking loss weight λ for the Annual-YBI model (DBSCAN spatial grouping). The red dot indicates the selected value (λ = 0.4), which achieved the best overall performance across six evaluation metrics.

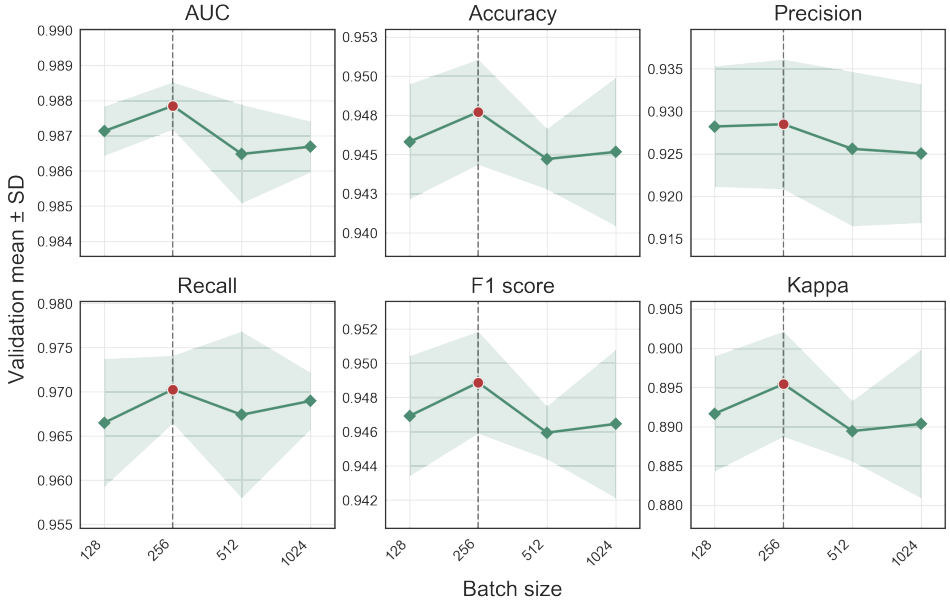

Fig. S6 Sensitivity of five-fold cross-validation performance to batch size for the Annual-YBI model (DBSCAN spatial grouping). A batch size of 256 was selected for final model training as it provided stable and optimal performance.

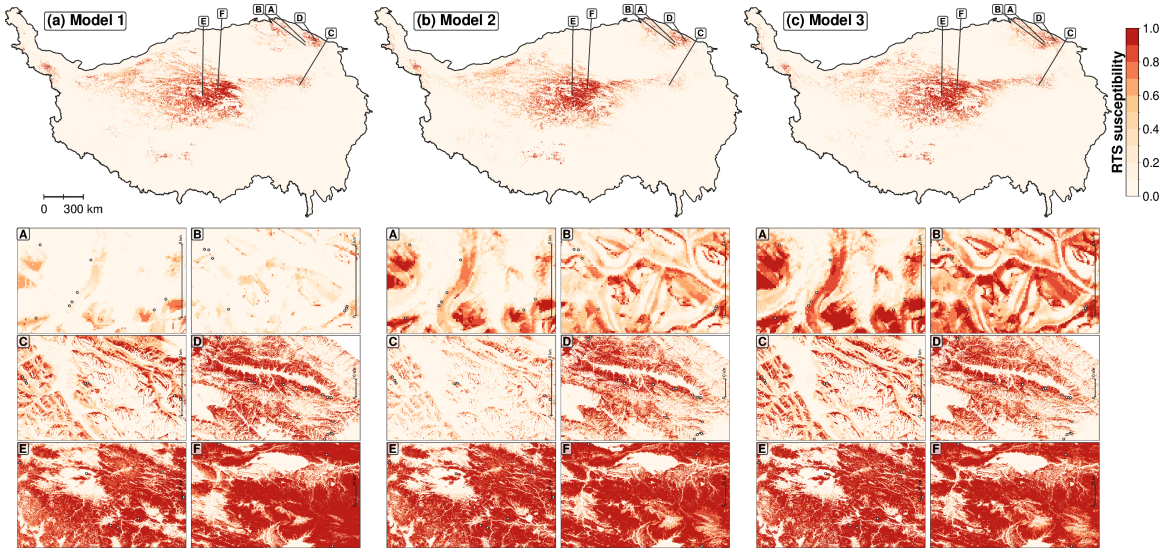

Fig. S7 Predicted RTS susceptibility maps for 2021 generated by (a) Model 1 (Static Binary), (b) Model 2 (Annual Binary), and (c) Model 3 (Annual-YBI). The upper row shows the full permafrost region of the QTP for each model. The lower panels display six zoomed-in sub-regions (A–F) highlighting differences in spatial detail and pattern among the three modeling approaches. The color scale represents predicted susceptibility from 0 (low) to 1 (high).

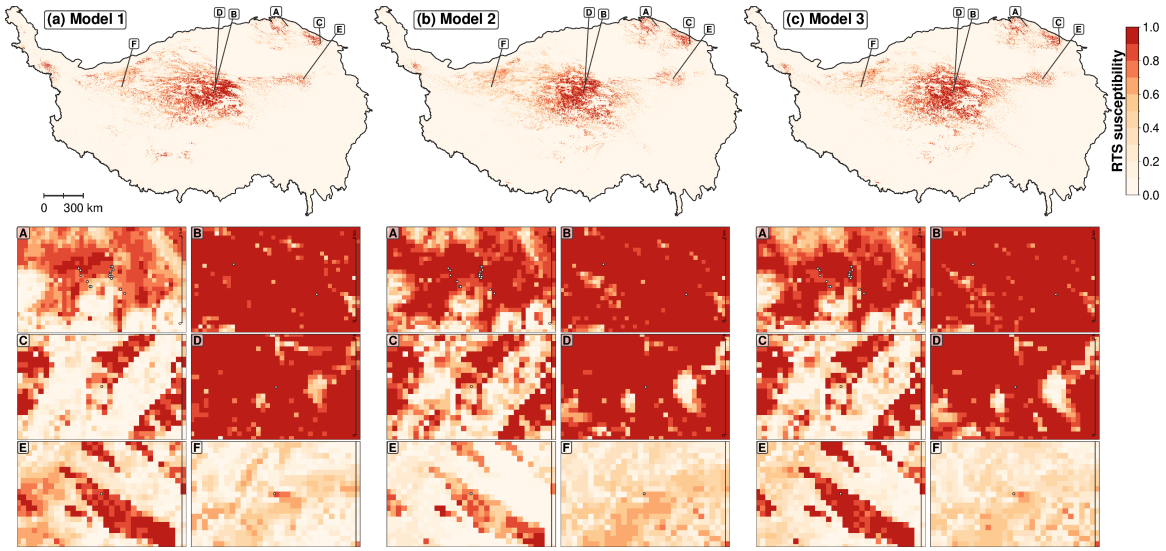

Fig. S8 Predicted RTS susceptibility maps for 2022 generated by (a) Model 1 (Static Binary), (b) Model 2 (Annual Binary), and (c) Model 3 (Annual-YBI). The layout and six zoomed-in sub-regions (A–F) are identical to those in Fig. S7. The color scale represents predicted susceptibility from 0 (low) to 1 (high).

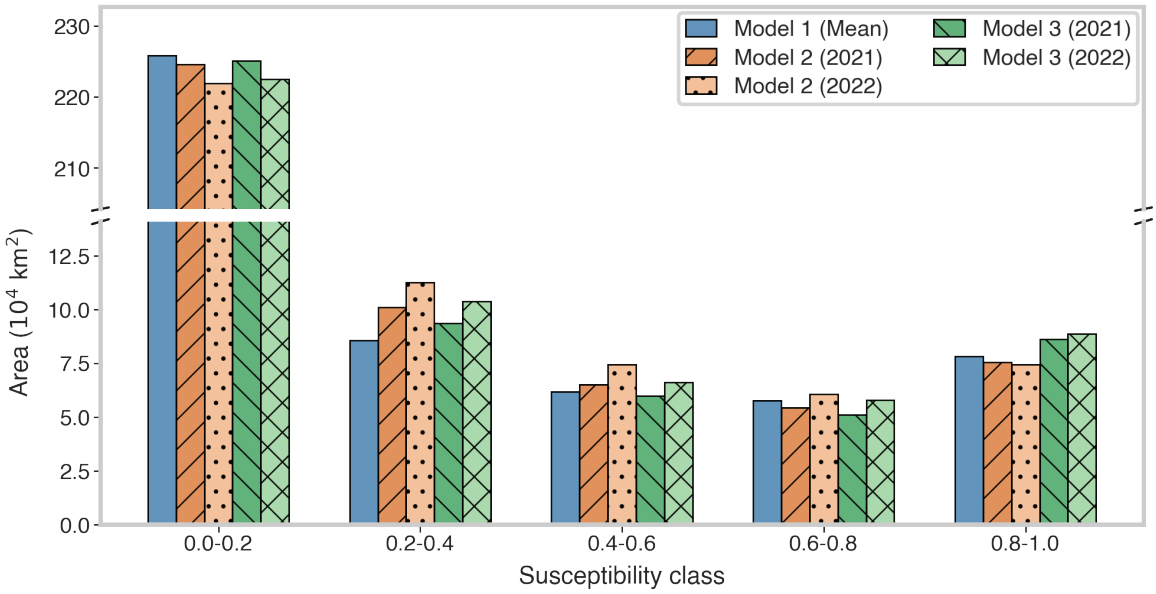

Fig. S9 Area distribution of predicted susceptibility classes for the three models in 2021 and 2022.

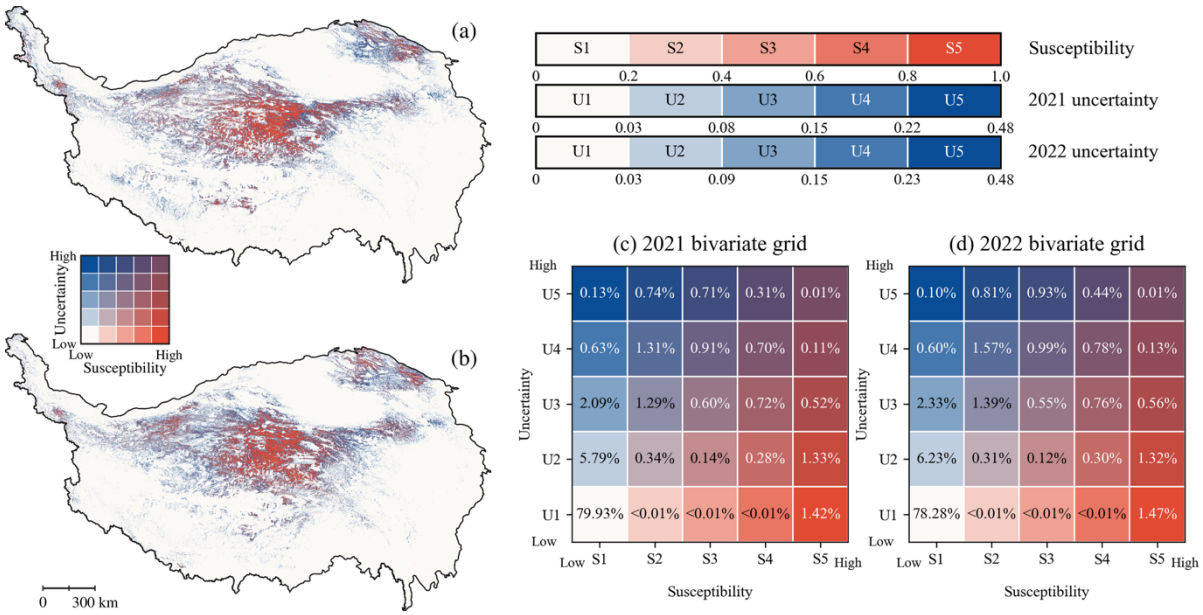

Fig. S10 Bivariate maps showing the spatial intersection of RTS susceptibility and prediction uncertainty for 2021 (a) and 2022 (b). The maps display 25 combined classes derived from five susceptibility levels (S1–S5) and five uncertainty levels (U1–U5). Color grids indicate the percentage of the permafrost area falling into each susceptibility–uncertainty combination for 2021 (c) and 2022 (d).

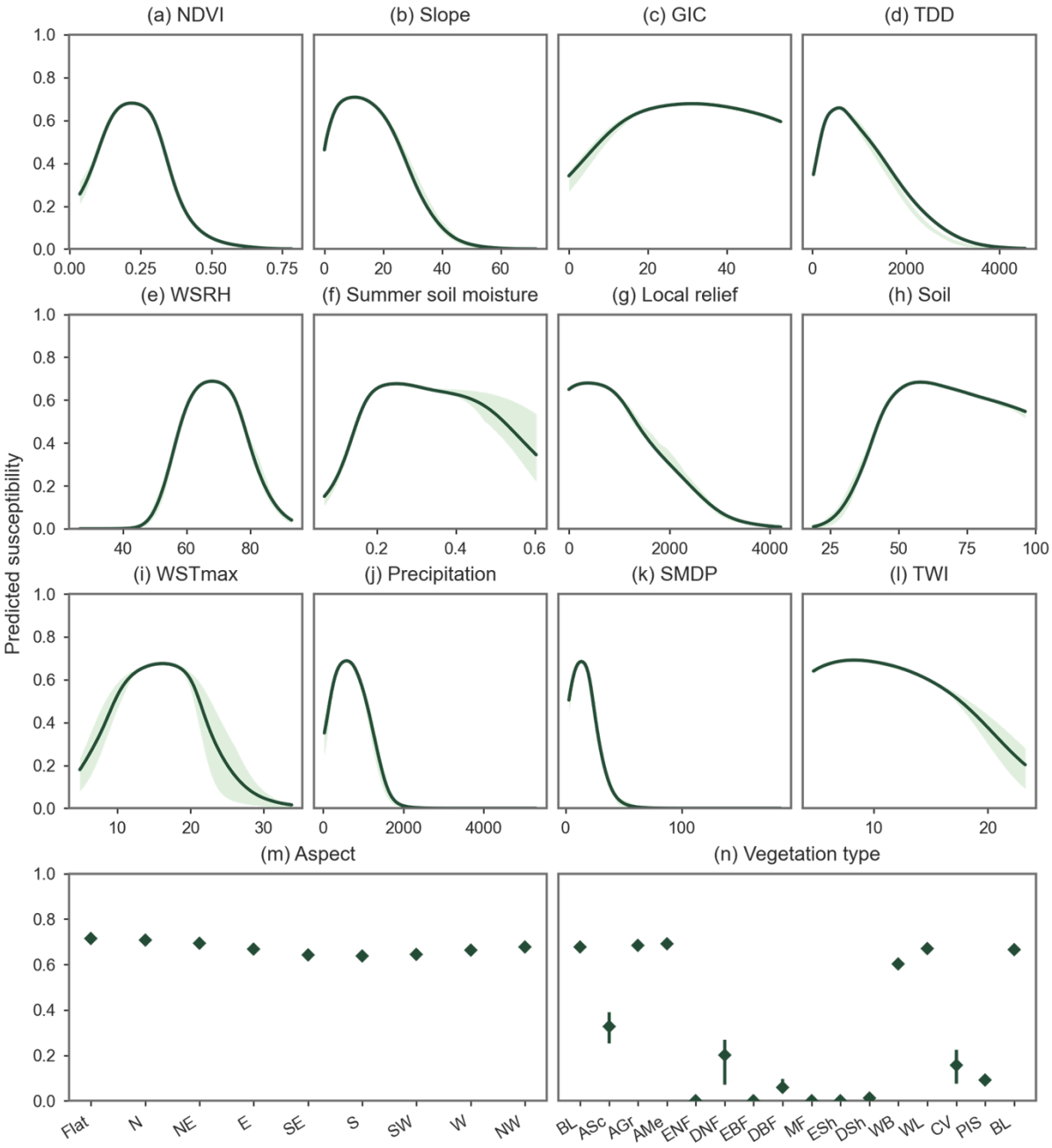

Fig. S11 SHAP dependence plots showing the marginal effects of individual predictors on predicted RTS susceptibility. Each panel displays the relationship between a single predictor and the model output while holding other variables constant. Green lines represent smoothed trends.